

[DT]

Induced compositional layering in a convecting fluid layer by an endothermic phase transition

Stuart A. Weinstein

Department of Geological Sciences, 1006 C. C. Little Building, University of Michigan, Ann Arbor MI, 48109, USA

Received January 10, 1992; revision accepted July 17, 1992

ABSTRACT

An endothermic phase change in the presence of chemical heterogeneities can act as an efficient filter, such that heavy material is sequestered below the phase change and light material is trapped above the phase change. Due to the fact that the endothermic phase change damps thermal convection, it can act as a “trap door” for chemical heterogeneities. Ascending flows which are chemically dense will need more thermal buoyancy to rise through the transition than ascending flows whose composition is closer to the background composition. Likewise, descending flows which are chemically light need more thermal buoyancy to sink through the transition. The results of a suite of numerical calculations of two-dimensional, double diffusive convection in a fluid layer with an endothermic phase change suggests that, if the 670 km seismic discontinuity has a steep enough Clapeyron slope, compositional layering may be induced and dynamically maintained by the transition. Furthermore, these calculations also show that the phase change and compositional boundaries will approximately coincide.

Introduction

The large-scale structure of thermal convection in the Earth's mantle may depend heavily on the nature of the 670 km seismic discontinuity. If the 670 km discontinuity is the result of a strongly endothermic phase transition and/or compositional boundary, whole-mantle convection may be suppressed and separate, but strongly coupled, convecting systems may develop above and below the 670 km discontinuity.

Experimental petrology and seismology provide evidence suggesting the 670 km discontinuity is either the result of a phase change or a change in the bulk composition of the mantle. High pressure and temperature laboratory experiments [1–4] performed on olivine support the hypothesis

that the 670 km discontinuity results from the olivine–spinel → olivine–perovskite + magnesio-wüstite phase transition. Analyses of body wave travel times suggest some subducting lithosphere extends through the 670 km discontinuity [5–8]. Other travel time studies indicate that the deflection of the 670 km discontinuity is at most a few tens of kilometers [9,10]. Both of these observations also support the phase change hypothesis.

However, in trying to reconcile mantle mineralogy with seismic velocity variations in the mantle several authors [e.g., 11–14] suggest that the lower mantle may be enriched in Fe compared to the upper mantle. As a result, the lower mantle may be 1–5% denser than the upper mantle. This evidence suggests interpreting the 670 km discontinuity as a compositional boundary. Still other studies [11,15–18] suggest that the 670 km discontinuity is the result of both a phase change and a change in the bulk chemistry of the mantle. Although slab penetration and stratification of the mantle remain highly controversial [19–23] the

Correspondence to: S.A. Weinstein, Department of Geological Sciences, 1006 C.C. Little Building, University of Michigan, Ann Arbor MI, 48109, USA.

data compiled so far allow for the possibility that the 670 km discontinuity is a combined compositional and phase change. Such a structure could arise in several ways; it may be a relic from differentiation in the early Earth [24], the phase change may be strongly dependent on composition, or it may result from a process of continuing differentiation where an endothermic phase change serves as a geochemical filter [25]. This study investigates the latter possibility and shows that, if a strong endothermic phase transition occurs at 670 km depth, it could induce a compositional boundary in the mantle that is approximately coincident with the phase transition.

The study of the effects of phase changes and compositional variations on thermal convection has a long history in geodynamics [e.g. 26–28]. In a comprehensive study, Christensen and Yuen [29] examined the effects of endothermic and exothermic phase transitions and showed how an endothermic phase change with a sufficiently steep Clapeyron slope can cause a transition to two-layer convection. This effect has recently been corroborated [30–32].

Both numerical and laboratory studies have been used to examine the effects of chemical stratification on thermal convection. Laboratory studies by Kincaid and Olson [33,34], Olson [35] and numerical studies by Christensen and Yuen [36], Christensen [37], and Kellogg [38] show that a density contrast between the upper and lower mantle of only 2–3% may be sufficient to induce two-layer convection in the mantle. Only Christensen and Yuen [36] considered the effects of a joint compositional–phase change boundary. They found the phase change and compositional boundaries coincided in some instances. In their study the fluid was initially simply stratified and the equilibrium positions of the phase change and compositional boundaries coincided, thus an endothermic phase change can maintain an existing compositional stratification [36]. This study addresses the issue of whether or not an endothermic phase transition can induce chemical layering giving rise to a compositional boundary.

The present study is different from that of Christensen and Yuen [36] in two important aspects. This study focuses on how endothermic phase changes can precipitate compositional layering, whereas Yuen and Christensen [36] con-

centrated on how phase changes and compositional boundaries affected subducting slabs. Furthermore, the calculations in this study start from an initial state in which the fluid is stratified in an unstable manner and does not contain any sharp compositional gradients. Any compositional boundaries that develop during the course of the calculation result from the interaction of thermochemical convection with the endothermic phase transition.

Model

The model system is two-dimensional, double diffusive convection in a fluid layer with an endothermic phase transition. The fluid layer is assumed to be Newtonian, Boussinesq, isoviscous and heated from below. In this model, the composition of the fluid is a mixture of two components; one dense and the other light. The location of the phase transition is assumed to depend on the temperature and depth (pressure) in the fluid, and the Clapeyron slope, but not on the composition of the fluid. The latter assumption appears to be justified if the olivine in the mantle is at least 75% forsterite end member [3,39].

The phase change formulation follows Richter [28] and Christensen and Yuen [29] such that the phase change is divariant and occurs over a finite depth interval. The phase of the fluid is represented by the continuous field, $\Gamma(x, z)$, which is a function of the reduced pressure Π :

$$\Gamma(x, z) = \frac{1}{2} \left(\tan H \left(\frac{\Pi}{d} \right) + 1 \right) \quad (1)$$

where:

$$\Pi = P - P_\tau \quad (2)$$

and P = pressure. P_τ is the transition pressure given by the Clapeyron equation:

$$P_\tau = P_o + \gamma T \quad (3)$$

(see Table 1 for symbol definitions). Here, P_o = zero temperature transition pressure; γ = the Clapeyron slope and T = temperature. If we ignore the non-hydrostatic pressure then:

$$\Pi = \rho_o g z_o - \rho_o g z - \gamma T \quad (4)$$

where: ρ_o = the density at the surface; g = the acceleration of gravity; z_o = the zero temperature transition depth.

TABLE 1

Definition of symbols

Symbols	Definitions
α	Thermal expansion coefficient
β	Concentration coefficient
γ	Clapeyron slope
γ^*	Dimensionless Clapeyron slope
κ	Thermal diffusivity
κ_c	Concentration diffusivity
ν	Kinematic viscosity
ρ	Density
ρ_o	Density at surface
$\Delta\rho_t$	Density change due to transition
ω_y	Vorticity
Δ	Aspect ratio
Γ	Phase function
Π	Reduced pressure
Ψ	Streamfunction
g	Acceleration of gravity
t	Time
x	Horizontal coordinate
z	Vertical coordinate
z_o	Zero T transition depth
C	Concentration
D	Fluid layer thickness
P	Pressure
P_o	Zero T transition pressure
P_t	Transition pressure
T	Temperature
ΔT	Temperature change
d	Transition width constant

Scaling the height z by D , the layer thickness, and γ by $(\rho_o gD)/\Delta T$, we obtain the dimensionless equation:

$$\Pi = z_o - z - \gamma^* T \quad (5)$$

where γ^* is the dimensionless Clapeyron slope. Γ ranges from a value of 0 for the low pressure

TABLE 2

Grid densities

γ^*	R_c	Coarse grid	Fine grid
Grid densities for $\Delta = 1$, $R_a = 100,000$ and $Le = 25$			
0.0	125,000	71 × 71	181 × 181
-0.09	125,000	71 × 71	141 × 141
-0.175	125,000	71 × 71	141 × 141
-0.2	125,000	71 × 71	141 × 141
-0.225	125,000	71 × 71	141 × 141
-0.3	125,000	71 × 71	121 × 121
-0.225	25,000	71 × 71	121 × 121
-0.225	325,000	71 × 71	141 × 141
Grid densities for $\Delta = 5$, $R_a = 100,000$ and $Le = 50$			
-0.15	125,000	351 × 71	1001 × 201
-0.20	125,000	351 × 71	1001 × 201
-0.25	125,000	351 × 71	1001 × 201
Grid densities for $\Delta = 1$, $R_a = 1,000,000$ and $Le = 80$			
0.0	1,000,000	87 × 87	451 × 451
-0.1	1,000,000	87 × 87	451 × 451
-0.2	1,000,000	87 × 87	451 × 451
-0.2	-1,000,000	87 × 87	451 × 451

Note: Grid densities are given as horizontal by vertical points.

phase to a value of 1 for the high pressure phase. The width of the transition is controlled by the constant d . For the calculations presented in this study $d = 0.05$.

The equation of state used in deriving the momentum balance equation has the form:

$$\rho = \rho_o(1 - \alpha T) + \beta C + \Gamma \Delta\rho_t \quad (6)$$

where the concentration, C , represents the fraction of the denser component fluid. Since the flow is two-dimensional, the momentum equation can be written in terms of Poisson equations for the streamfunction and vorticity. Using D^2/κ , ΔT , and ΔC , for time, temperature and concen-

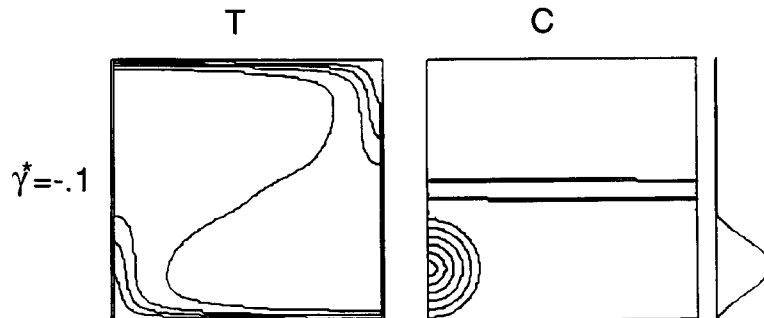


Fig. 1. Initial temperature and concentration fields used for calculations performed with $R_a = 10^6$, $R_p = 2 \times 10^6$, $Le = 80$, $\Delta = 1$ and a spatially restricted, initial chemical heterogeneity.

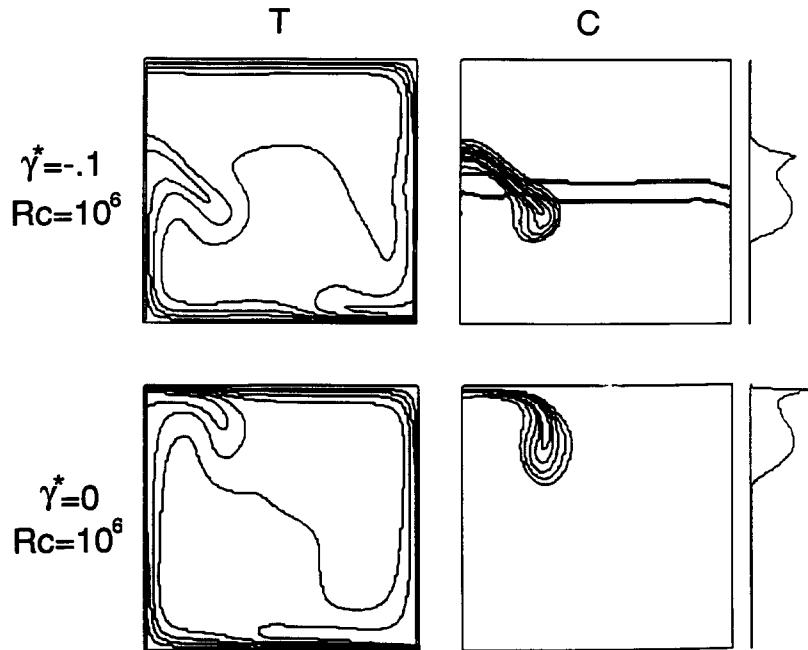


Fig. 2. The effects of negative γ^* on the ability of an ascending plume to transport chemical heterogeneity across a phase transition. The graph to the right of the concentration fields shows the horizontally averaged concentration. In these calculations $R_a = 10^6$, $R_c = 10^6$, $R_p = 2 \times 10^6$, $Le = 80$ and $\Delta = 1$.

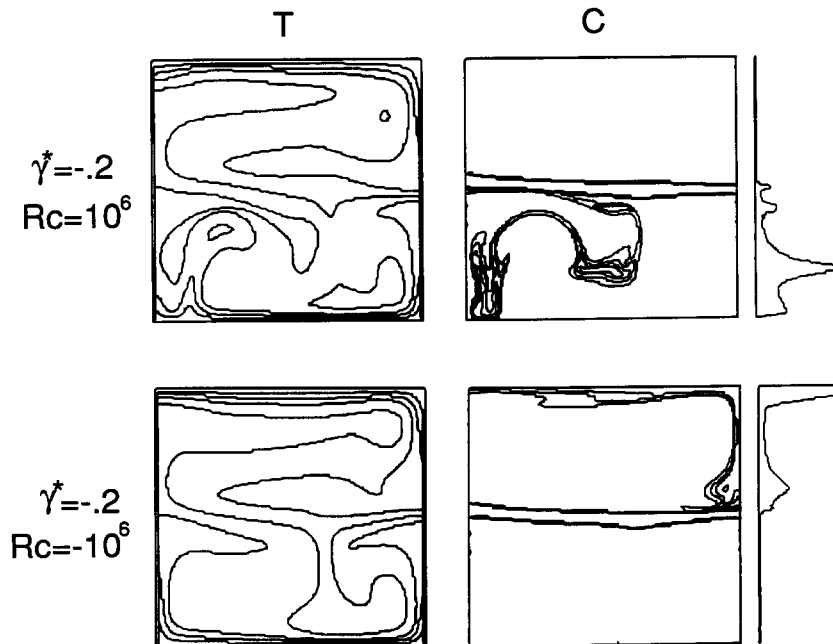


Fig. 3. The effects of dense ($R_c = 10^6$) and light ($R_c = -10^6$) heterogeneity on the ability of an ascending plume to transport chemical heterogeneity across a phase transition. In these calculations $R_a = 10^6$, $R_p = 2 \times 10^6$, $\gamma^* = -0.2$, $Le = 80$ and $\Delta = 1$.

tration scales, the dimensionless Poisson equations for vorticity and streamfunction are:

$$\nabla^2 \omega_y = R_a \left(1 + \frac{R_p}{R_a} \gamma^* \frac{d\Gamma}{d\Pi} \right) \frac{\partial T}{\partial x} - R_c \frac{\partial C}{\partial x} \quad (7)$$

$$\nabla^2 \Psi = \omega_y \quad (8)$$

where Ψ and ω_y = the streamfunction and vorticity, respectively. R_a , R_p and R_c are the thermal, phase change and chemical Rayleigh numbers and have the following definitions:

$$R_a = \frac{g\alpha\Delta TD^3}{\kappa\nu} \quad R_p = \frac{g\Delta\rho_\tau D^3}{\rho_o\kappa\nu} \quad R_c = \frac{g\beta\Delta CD^3}{\kappa\nu} \quad (9)$$

The dimensionless advection–diffusion equations for heat and concentration are:

$$\frac{\partial T}{\partial t} + J(\Psi, T) = \nabla^2 T \quad (10)$$

$$\frac{\partial C}{\partial t} + J(\Psi, C) = \frac{1}{Le} \nabla^2 C \quad (11)$$

where $Le = \kappa/\kappa_c$ is the Lewis number. The latent heat term due to the phase change scales with the dissipation number and is therefore not present in the Boussinesq limit [29].

All of the fluid boundaries are assumed to be stress-free and impermeable. In addition, the top and bottom boundaries are isothermal and the sidewalls are insulating. With respect to concen-

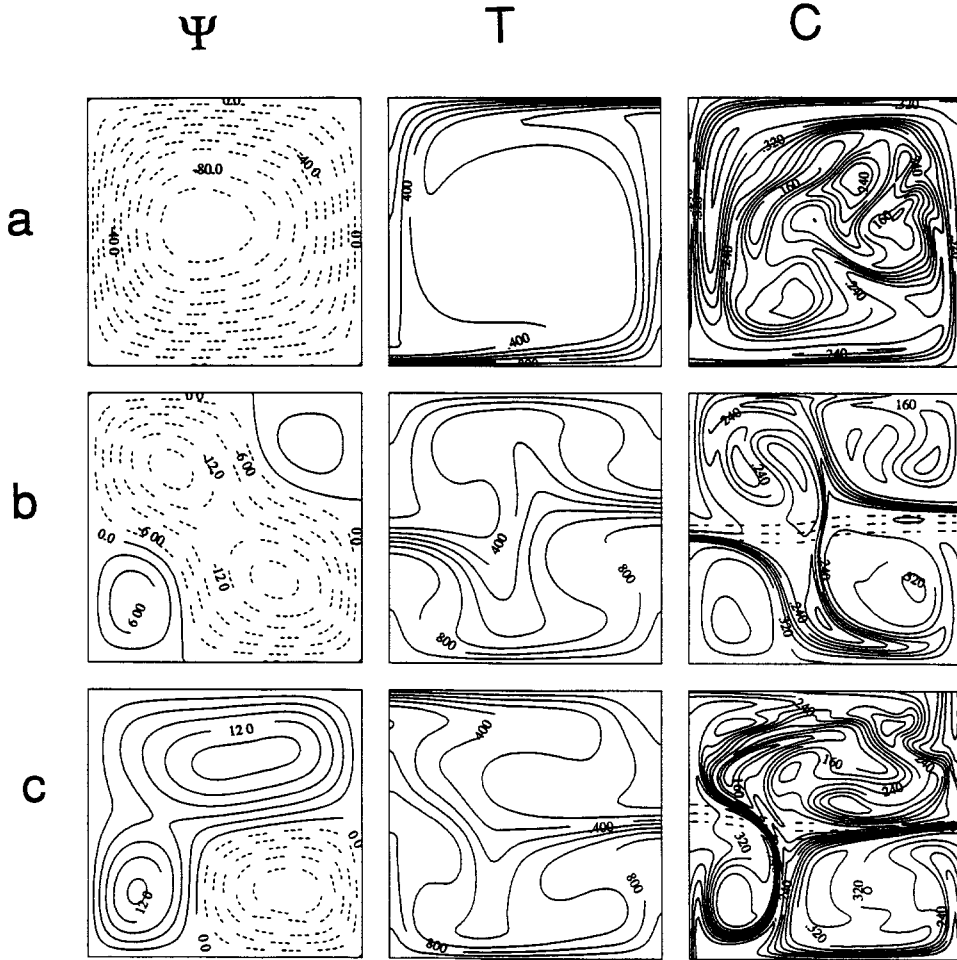


Fig. 4 Streamfunction, temperature and concentration fields obtained in square box calculations at a dimensionless time of 0.042 $R_a = 10^5$, $R_p = 2R_a$, $R_c = 1.25R_a$ and $Le = 25$ (a) $\gamma^* = 0.0$ (b) $\gamma^* = -0.09$. (c) $\gamma^* = -0.175$

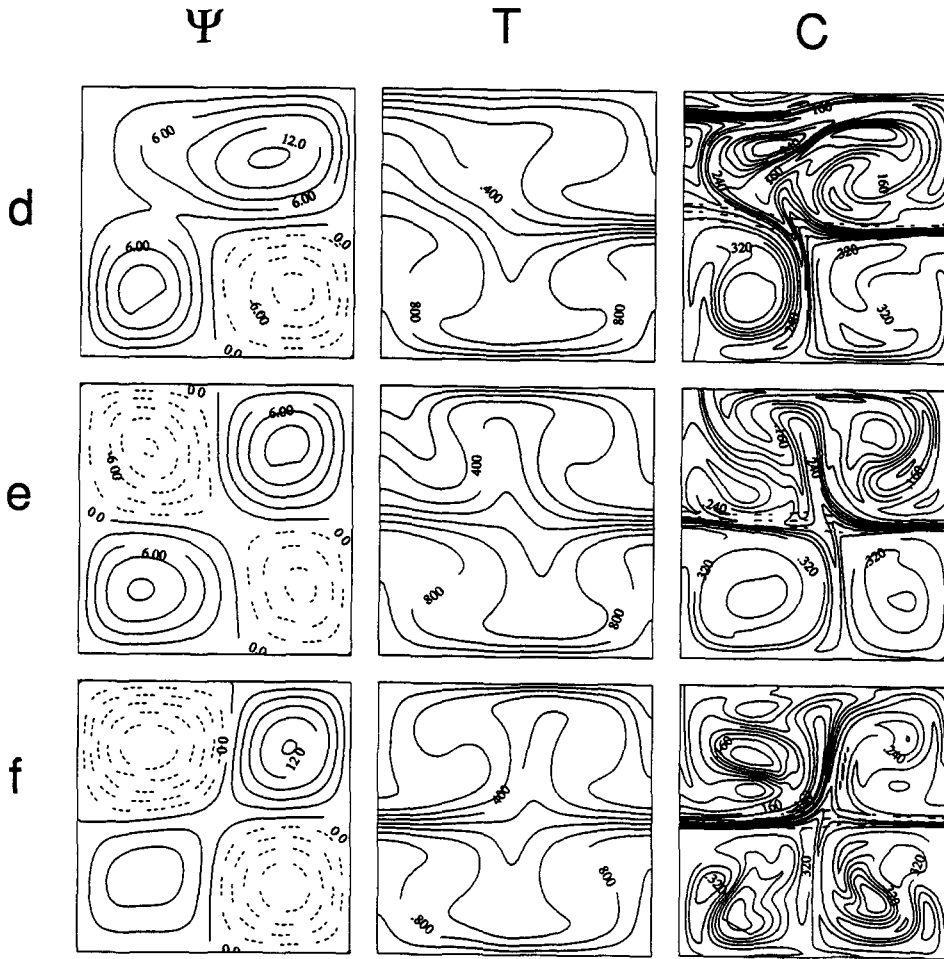


Fig. 4 (continued). (d) $\gamma^* = -0.2$. (e) $\gamma^* = -0.225$ (f) $\gamma^* = -0.3$.

tration, all boundaries are insulating. In terms of Ψ , ω_y , T , and C , the boundary conditions are:

$$\Psi = \omega_y = T = \frac{\partial C}{\partial z} = 0 \quad [z = 1] \quad (12)$$

$$\Psi = \omega_y = \frac{\partial C}{\partial z} = 0 \quad T = 1 \quad [z = 0] \quad (13)$$

$$\Psi = \omega_y = \frac{\partial T}{\partial x} = \frac{\partial C}{\partial x} = 0 \quad [x = 0, \Delta] \quad (14)$$

Equations (7), (8), (10) and (11) are solved subject to the boundary conditions (12), (13) and (14) using the method of finite difference [40]. Since concentration diffuses much more slowly than heat, chemical boundary layers or plumes may be characterized by much smaller length scales than their thermal counterparts. As a re-

sult, the numerical resolution required by the concentration field is much greater than the resolution required by either the momentum or temperature field. In calculations where $Le = 80$, the concentration is computed on a mesh with a gridpoint interval one fifth as large as that used for Ψ , ω_y and T . In each time step, Ψ is interpolated onto the fine mesh with bi-linear splines and used to advect the concentration. After the concentration field has been updated, it is interpolated (also using bi-linear splines) onto the coarse mesh used in calculating Ψ , ω_y and T . The numerical scheme conserves mass to 1 part in 10^6 . The grid densities used for the calculations can be found in Table 2.

The principal limitations of the calculations performed in this study are the small values of Le

and the assumption of no internal heating. Hoffman and Hart [41] estimated κ_c for the mantle to be $10^{13} \text{ cm}^2 \text{ sec}^{-1}$. This implies Le for the mantle may be as large as 10^{11} and, therefore, the effects of chemical diffusion are not expected to be important in mantle convection. The low values of Le used in these calculations reflect the limitations of the numerical method. However, as long as the duration of the calculation is considerably less than a thermal diffusion time ($t < 0.05$), the effects of chemical diffusion are probably unimportant [42].

Two basic types of numerical experiments are considered in this study. The first type examines

the behavior of the numerical model when the heterogeneity is initially restricted to a small region, (i.e., confined to a slab or D''). The second type of experiment examines the behavior of the numerical model when the heterogeneity is distributed throughout the fluid layer.

In the first set of experiments, the initial temperature field is taken from the early stage of convective spin up for a calculation where $R_a = 10^6$, $R_p = 2R_a$ and $\gamma = -0.1$ ($R_c = 0$). At this point the calculation is stopped and a small semi-circular region which contains the nascent ascending plume is made chemically heterogeneous from the rest of the fluid. The composition of the

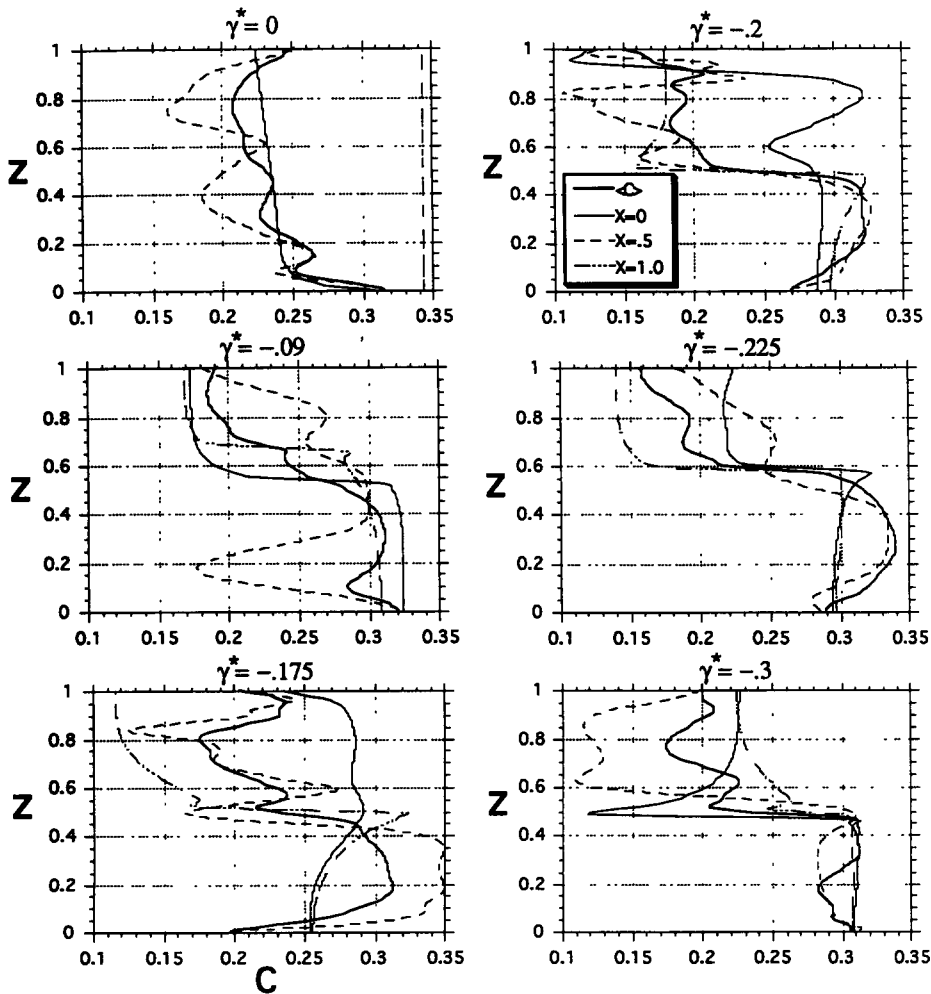


Fig 5 Vertical profiles of the concentration fields corresponding to Fig 4. The profiles are obtained from locations $x = 0, 0.5, 1.0$. $\langle C \rangle$ is the horizontally averaged concentration.

fluid in this region is given by:

$$C = \frac{0.375 * (0.2 - [x^2 + (z - 0.2)^2]^{0.5})}{0.2} + 0.1$$

This region is centered at $x = 0.0$, $z = 0.2$ and has a radius of 0.2. The fluid outside of this region has the composition $C = 0.1$.

For numerical experiments where the heterogeneity is initially distributed throughout the fluid layer, the concentration field is given the initial distribution:

$$C = 1.5(1 - z)z$$

In a square box ($\Delta = 1$) the initial momentum and temperature field consist of a single cell

perturbation with top and bottom thermal boundary layers. In the long box calculations ($\Delta = 5$) the initial condition consists of three cells with aspect ratios of 1.0, 3.0, and 1.0, from left to right. The equilibrium position of the phase change is assumed to be $z = 0.5$. This combination of initial concentration distribution and equilibrium position (when convection is absent) of the phase change is selected because:

- (1) the same amount of concentration exists above and below the equilibrium position of the phase change;
- (2) the initial concentration distribution is gravitationally unstable;
- (3) there are no sharp gradients in the initial concentration distribution.

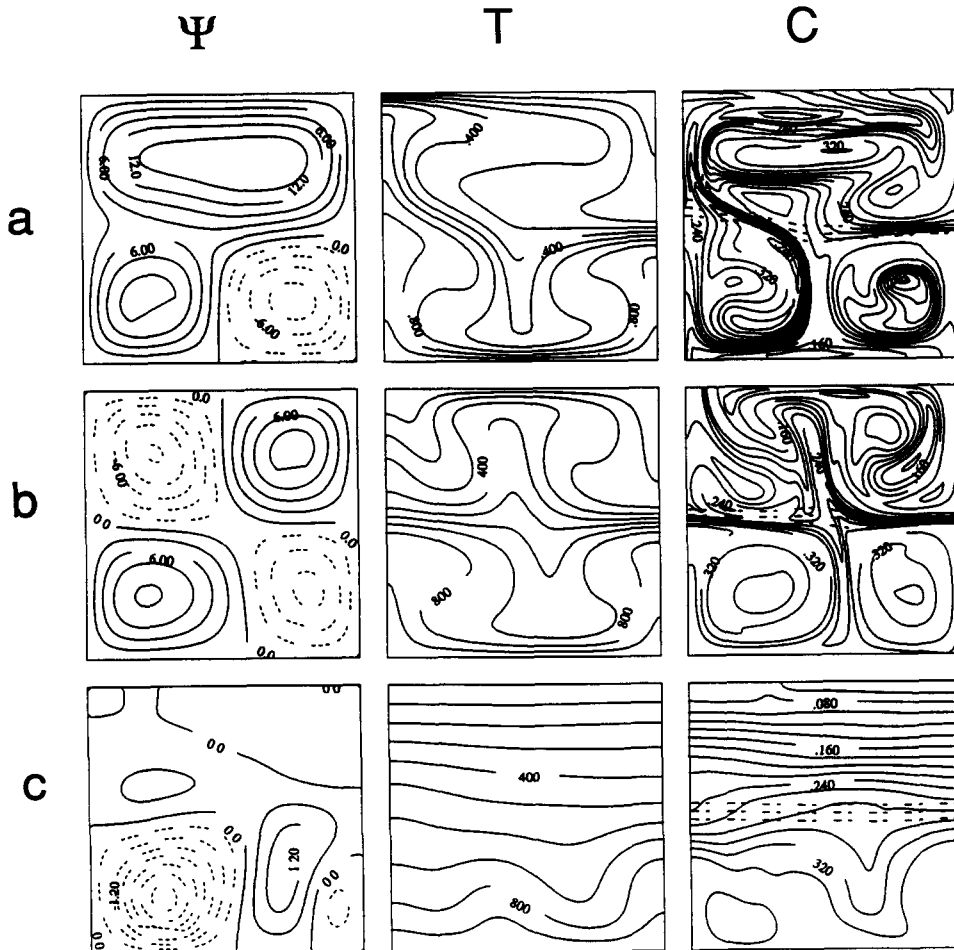


Fig. 6. Streamfunction, temperature and concentration fields obtained in square box calculations at a dimensionless time of 0.042. $R_a = 10^5$, $R_p = 2R_a$, $Le = 25$, $\gamma^* = -0.225$. (a) $R_c = 0.25R_a$, (b) $R_c = 1.25R_a$, (c) $R_c = 3.25R_a$.

Thus any sharp gradients which develop in the concentration field that are juxtaposed with the phase transition are due to the dynamics of the system.

Results

In an effort to gain insight into the dynamics of our model, a number of calculations were performed in square boxes ($\Delta = 1$). The first series of experiments to be presented focus on one aspect of the filtering mechanism, the transport of chemical heterogeneity by plumes. The initial

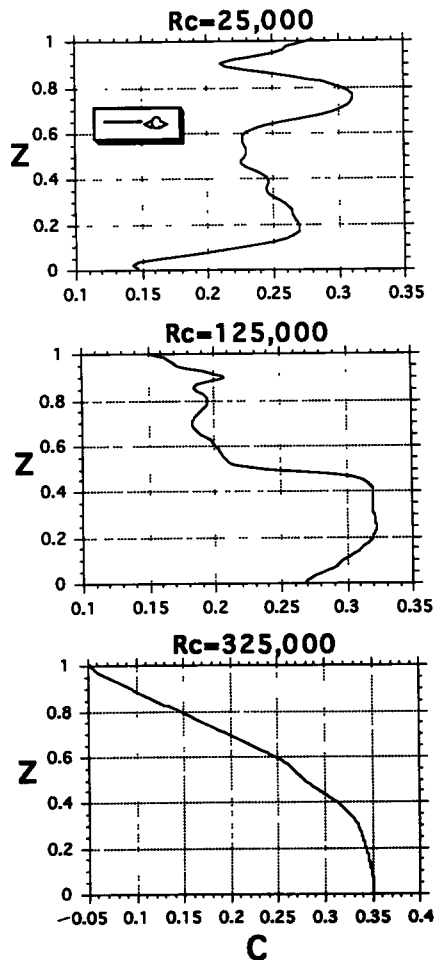


Fig. 7. Profiles of the horizontally averaged concentration fields corresponding to Fig. 6. $R_a = 10^5$, $R_p = 2R_a$, $Le = 25$, $\gamma^* = -0.225$. (a) $R_c = 0.25R_a$. (b) $R_c = 1.25R_a$. (c) $R_c = 3.25R_a$.

conditions for these calculations were discussed in the model section and are clarified by Fig. 1.

The first two experiments were performed for the same values of R_c , R_a and R_p (10^6 , 10^6 , 2×10^6) but with differing values of γ^* (0 , -0.1). The temperature and concentration fields for these calculations are shown in Fig. 2. The two sub-horizontal lines near the middle of the box in the concentration field are the 0.2 and 0.8 contours of Γ and indicate the position of the transition region. When $\gamma^* = 0$ (no phase transition) the heterogeneity is transported to the top of the fluid layer. In the absence of the phase change the plume has enough thermal buoyancy to overcome the opposing, compositional buoyancy of the heterogeneity. However, when $\gamma^* = -0.1$, the ascending plume is no longer able to transport all of the heterogeneity across the fluid layer and much of the heterogeneity is trapped beneath the phase transition.

The next two experiments show the system after 1–2 overturns have elapsed. The values of R_a , R_p and γ^* for these experiments are held fixed with the values 10^6 , 2×10^6 and -0.2 respectively, and $R_c = 10^6$, -10^6 . The temperature and concentration fields for these calculations are shown in Fig. 3. In the case where $R_c = 10^6$, the ascending plume is stopped by the phase transition and the heterogeneity is not transported across the phase transition. However, in the case where $R_c = -10^6$, the heterogeneity is less dense than the surrounding fluid and assists the plume in transport across the phase transition. The resulting situation is the opposite of the previous case. Here, the heterogeneity is trapped above the phase transition and, in effect, has been filtered out of the lower layer.

In the next series of calculations the chemical heterogeneity is distributed throughout the fluid layer. The values of R_a , R_p and R_c are 10^5 , 2×10^5 and 1.25×10^5 , respectively and $Le = 25$. The only parameter which is varied is γ^* . In these calculations convection is time-dependent and, therefore, the calculations are compared to one another by showing snapshots of the T , Ψ and C fields at the same dimensionless time, $t = 0.042$. This time was chosen because of the low value of Le ; however, in all cases where compositional layering develops it occurs quickly, usually within 2 or 3 overturns.

The results of six square box calculations are displayed in Fig. 4. The value of γ^* decreases from zero in Fig. 4a to -0.3 in Fig. 4f. In the case where γ^* is zero, the phase transition is absent and thermal convection is strong enough to mix the concentration field. However, as γ^* is decreased, a system of layered convection develops and sharp compositional gradients occur in close proximity to the phase transition. The position of the phase transition is denoted by three dashed lines representing, from top to bottom,

the 0.2, 0.5 and 0.8 contours of Γ . For $\gamma^* < -0.09$, these contours bracket the sharp, vertical compositional gradients which have developed near the middle of box. It is evident that, unless two-layer convection is produced, vertical concentration gradients cannot be expected to form in close proximity to the phase transition.

To highlight the distribution of concentration further, vertical profiles of the concentration field at three horizontal locations as well as the horizontally averaged concentration ($\langle C \rangle$) are



Fig 8 Streamfunction fields obtained in a long box calculation ($\Delta = 5$) at dimensionless times of (a) 0.0103, (b) 0.022, (c) 0.032, (d) 0.044. $R_a = 10^5$, $R_p = 2R_a$, $R_c = 1.25R_a$, $\gamma^* = -0.2$, $Le = 50$

shown in Fig. 5 for the same concentration fields of Fig. 4. In the case where γ^* is zero the concentration is nearly evenly distributed through the entire box. However, when γ^* is decreased from zero, the concentration becomes more abundant in the lower half of the box, below the endothermic phase transition. Clearly, the endothermic phase transition acts as a filter for the concentration. Fluid parcels rich in concentration (heavier) need greater thermal buoyancy in order to rise through the phase transition and therefore

these fluid parcels are preferentially separated from lighter fluid (low in concentration) at the phase transition.

Figure 6 shows the effect of varying R_c while leaving R_a , R_p and γ^* fixed. In these calculations $R_a = 10^5$, $R_p = 2 \times 10^5$ and $\gamma^* = 0.225$ and $R_c = 0.25R_a$, $1.25R_a$ and $3.25R_a$ in Figs. 6a-c, respectively. When R_c is small, the concentration behaves almost as if it were a passive tracer. In this limit the filter mechanism discussed above has little to filter out because variations in density

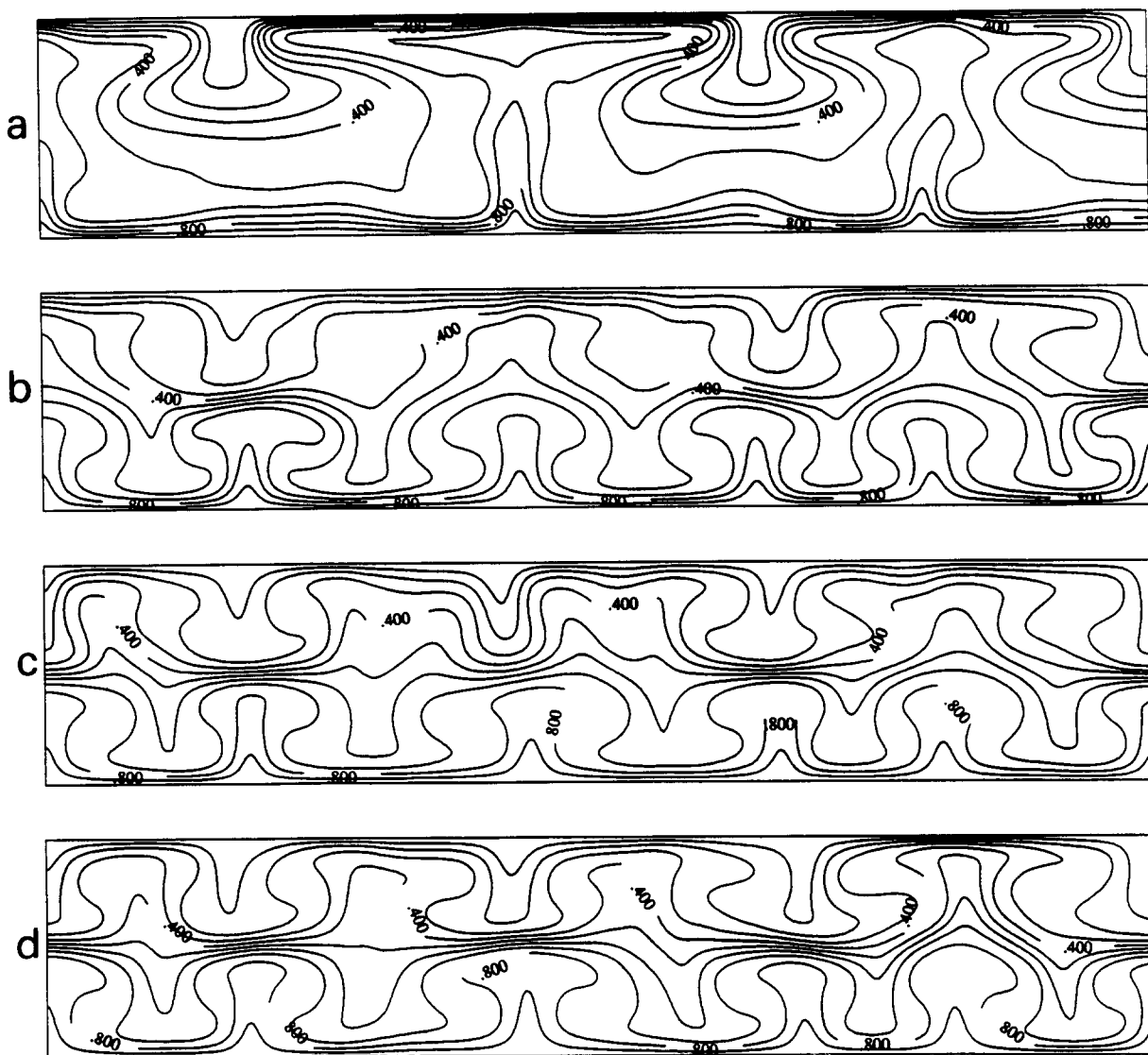


Fig. 9. Temperature fields obtained in a long box calculation ($\Delta = 5$) at dimensionless times of (a) 0.0103, (b) 0.022, (c) 0.032, (d) 0.044. $R_a = 10^5$, $R_p = 2R_a$, $R_c = 1.25R_a$, $\gamma^* = -0.2$, $Le = 50$.

due to the concentration are much smaller and the compositional layering is therefore very weak. This is illustrated in Fig. 7a, which shows the vertical distribution of $\langle C \rangle$. Not only is a sharp change in $\langle C \rangle$ absent near the transition depth, but no discernable layering has developed either. When R_c is made large, the variations in density of the fluid due to the concentration overwhelm the thermal effects. In Fig. 6c, the fluid has become stratified and convection is decaying. The vertical distribution of $\langle C \rangle$ (Fig.

7c) shows the stratification; however, unlike the case where $R_c = 1.25R_a$ (Fig. 7b) no sharp gradients in $\langle C \rangle$ are present. The point of this calculation is to show that a sharp compositional boundary is not favored by the initial conditions. In the large R_c limit, heavy fluid (large C) will simply sink through the transition to the bottom of the layer. Flow driven by thermal buoyancy will not be strong enough to entrain this fluid and transport it to the phase boundary. Therefore, in the large R_c limit, the vertical concentration gra-

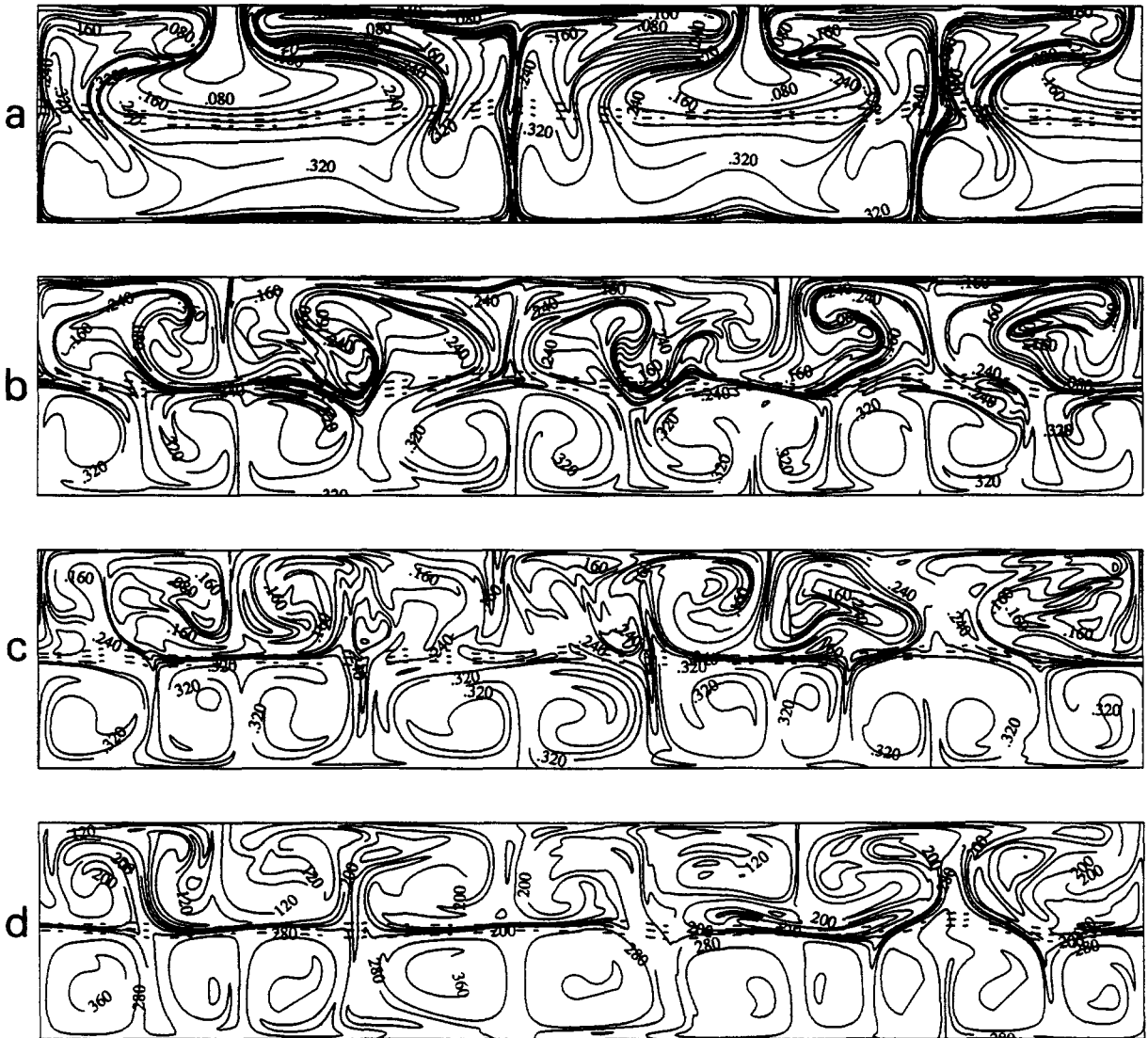


Fig. 10. Concentration fields obtained in a long box calculation ($D = 5$) at dimensionless times of (a) 0.0103, (b) 0.022, (c) 0.032, (d) 0.044. $R_a = 10^5$, $R_p = 2R_a$, $R_c = 1.25R_a$, $\gamma^* = -0.2$, $Le = 50$.

dients do not form either. The formation of vertical compositional gradients near an endothermic phase transition is not a general effect and occurs for only a specific range of values for the governing parameters.

Three calculations in a long box ($\Delta = 5$) were performed using $\gamma^* = -0.15, -0.2$ and -0.25 . The other parameters, R_a, R_p, R_c and Le are held fixed with values of $10^5, 210^5, 1.25 \times 10^5$ and 50. Only the evolution of the flow for the case $\gamma^* = -0.2$ will be discussed in detail.

Figures 8–10 show the evolution of the system when $\gamma^* = -0.2$. During the initial phase (Figs. 8a, 9a and 10a) ascending thermochemical plumes rise through the phase transition and pancake against the top of the fluid layer. Since these plumes are chemically light with respect to their surroundings, the chemical buoyancy reinforces the thermal buoyancy and drives the plumes up through the phase transition. Some entrainment

of chemically dense fluid ($C > 0.25$) across the transition occurs (Fig. 10a), however, much of this fluid is prevented from crossing the transition and begins to move downwards. The descending plumes are also chemically light, but in this case the chemical buoyancy opposes the thermal buoyancy. Unlike the ascending plumes, the descending plumes lack the requisite buoyancy needed to penetrate the phase transition. The filter effect of the endothermic phase transition is quite evident as chemically light fluid is sequestered above the transition and chemically dense fluid is trapped below. As the system evolves (Figs. 8b–d, 9b–d and 10b–d) a pattern of two-layer convection becomes dominant, and sharp vertical concentration gradients begin to appear near the phase transition, as do thermal boundary layers. By a dimensionless time of 0.044 (Fig. 10d) the vertical concentration gradients extend across the entire layer. Just as in the square box calculations, these

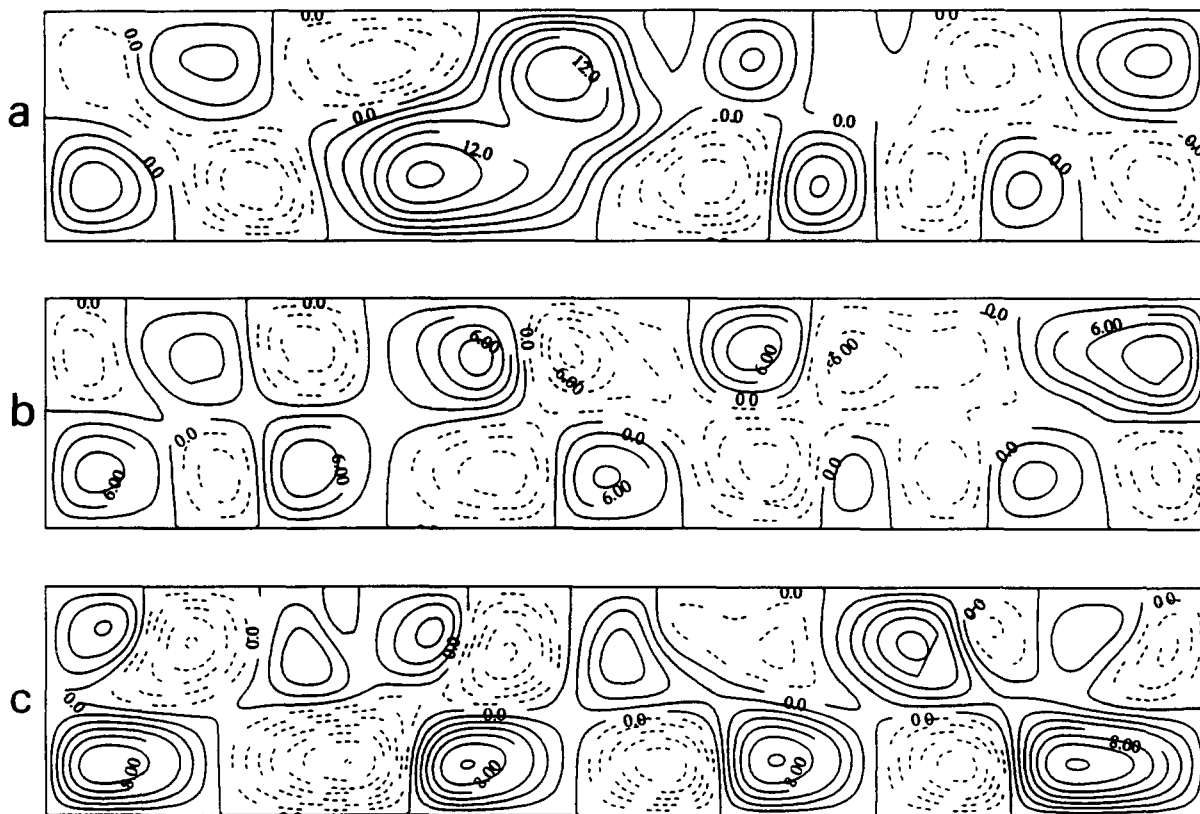


Fig. 11. Streamfunction fields obtained in a long box calculations ($D = 5$) at a dimensionless time of 0.032 for (a) $\gamma^* = -0.15$, (b) $\gamma^* = -0.2$, (c) $\gamma^* = -0.25$. $R_a = 10^5$, $R_p = 2R_a$, $R_c = 1.25R_a$, $Le = 50$.

gradients are bracketed by the 0.2 and 0.8 contours of Γ and, in most instances, completely cover the 0.5 contour which denotes the position of the phase boundary. When scaled to the thickness of the mantle, the compositional boundary (vertical concentration gradients) is within ± 40 km of the phase transition.

The streamfunction and concentration fields for $\gamma^* = -0.15, 0.2, 0.25$, at a dimensionless time of 0.032 are shown in Figs. 11 and 12. By this time, vertical concentration gradients have developed for both the $\gamma^* = -0.15, 0.2$ cases. The vertical concentration gradients are best developed for $\gamma^* = -0.2$. When $\gamma^* = -0.25$, the mass transfer across the transition is severely limited in comparison to the two previous cases. In this case, the vertical concentration gradients near the phase change are much weaker. Because the mass transfer across the phase transition is so reduced, the vertical gradients need more time to evolve. If

the Clapeyron slope is made so steep that the phase transition behaves like an impermeable boundary, the filtering mechanism is eliminated, and a jump in $\langle C \rangle$ will not occur, given the initial concentration distribution used in this study.

Discussion and conclusions

The suite of calculations presented in this study demonstrate the ability of an endothermic phase transition to induce a compositional boundary that is juxtaposed with the location of the phase change in a fluid layer undergoing thermochemical convection. In order for the compositional boundary to form, the Clapeyron slope must be steep enough to produce regions in the fluid where convection is layered. In addition, the variations in the fluid density due to changes in composition must be large enough so that the

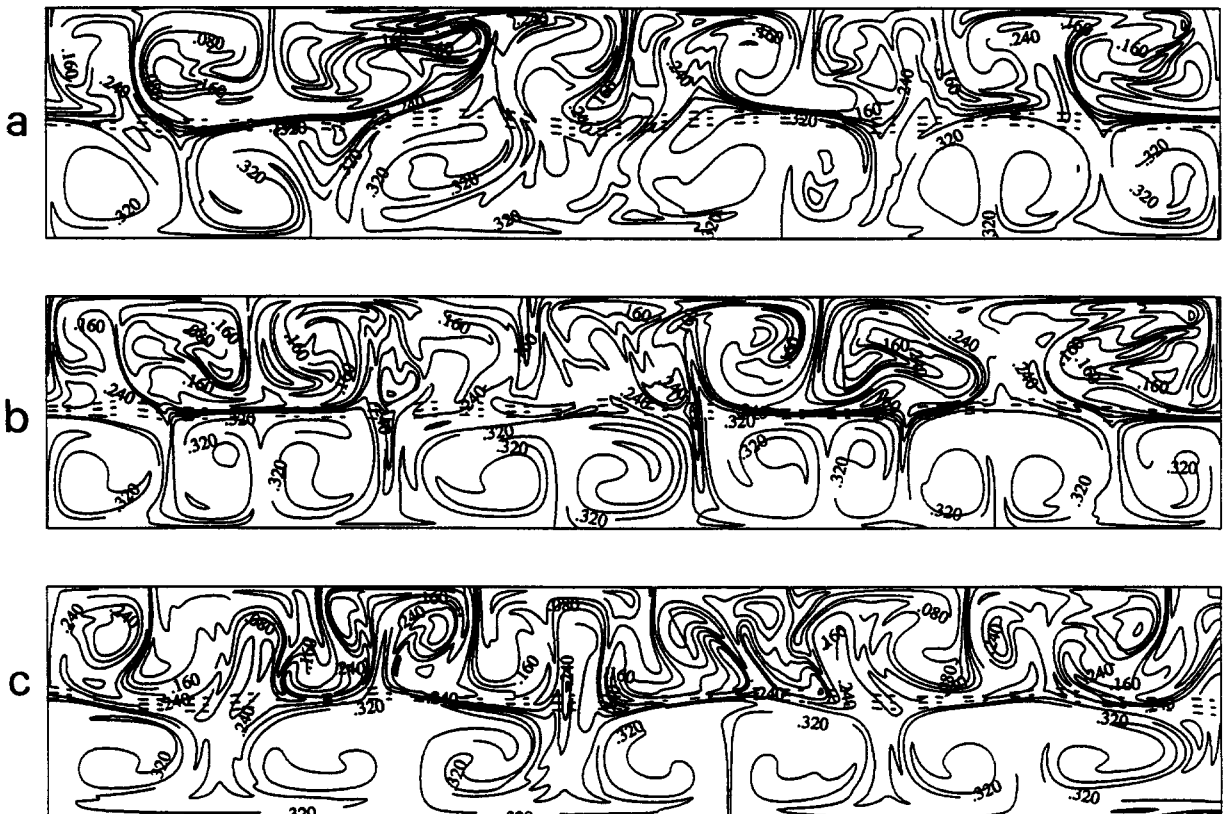


Fig. 12. Concentration fields obtained in a long box calculations ($D = 5$) at a dimensionless time of 0.032 for (a) $\gamma^* = -0.15$, (b) $\gamma^* = -0.2$, (c) $\gamma^* = -0.25$. $R_a = 10^5$, $R_p = 2R_a$, $R_c = 1.25R_a$, $Le = 50$.

separation of intrinsically light and dense fluid elements can occur. The square box calculations indicate that the development of a compositional boundary is most likely to occur when $R_c/R_a \sim 1.0$. When these criteria are met, the endothermic phase transition can become an efficient filter for long wavelength chemical heterogeneity. The long term evolution of the calculations in this study is not known because of their relatively short duration (1–3 overturns). It is possible that viscous entrainment across the phase transition could remix the layer via the formation of short wavelength heterogeneities, which cannot be subsequently filtered by the phase change.

The density variations due to changes in composition that are found in these numerical experiments can be estimated using the Rayleigh number ratio $R_c/R_a = (\beta \Delta C)/(\alpha \Delta T)$. Assuming typical values for α , ΔT , and ρ_0 of $2.0 \times 10^{-5} \text{ K}^{-1}$, 3000 K, and 3300 kg^{-3} , respectively, the density contrast between the heterogeneity and the surrounding fluid in the first set of experiments (Figs. 2 and 3) is, on average, 24.7 kg^{-3} (0.75%), with a maximum of 74.1 kg^{-3} (2.25%). Thus, the compositional density contrast between the heterogeneities used for the calculations presented in Fig. 3 is only 1.5% on average. This small density contrast made the difference in whether the ascending plume (bottom of Figs. 3 and 4) was trapped by or penetrated the phase transition.

In the long box experiments, the change in density which occurs across the phase transition can be estimated from Fig. 13. For $\gamma^* = -0.2$ and -0.15 , the change in concentration across the transition is approximately 0.15. Since $(R_c/R_a) = 1.25$, this figure represents a density contrast of 37 kg m^{-3} or a change in density of 1.1% across the transition due to the change in bulk composition. This is much lower than the 2–3% change in density across a compositional boundary needed to maintain two-layered convection. Here, the endothermic phase transition is primarily responsible for the layering of convection and the compositional boundary develops as a response to the phase transition.

The dimensionless group $(R_p/R_a)/\gamma^*$ can be used to determine the dimensional value of γ^* used in this study. Assuming a value of 0.11 for $(\Delta\rho_t)/\rho_0$ [43], $\gamma = -5.2 \text{ MPa K}^{-1}$, -6.9 MPa

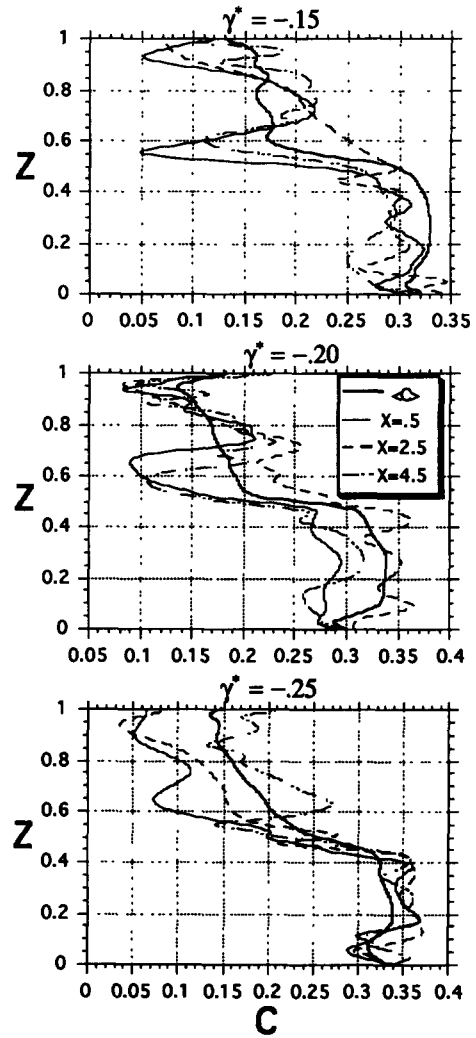


Fig. 13. Vertical profiles of the concentration fields for (a) $\gamma^* = -0.15$, (b) $\gamma^* = -0.2$, (c) $\gamma^* = -0.25$ at a dimensionless time of 0.032. The profiles are obtained at locations $x = 0.5, 2.5, 4.5$. $\langle C \rangle$ is the horizontally averaged concentration.

K^{-1} and -8.6 MPa K^{-1} for $\gamma^* = -0.15$, -0.2 and -0.25 , respectively. These values are on the high end of the experimentally determined range for γ of $-2.0 \text{ MPa K}^{-1} < \gamma < -7.0 \text{ MPa K}^{-1}$ for the spinel \rightarrow perovskite + magnesiowustite phase change [3,4]. However, Christensen and Yuen [29] showed that the transition to two-layer convection occurs for smaller values of $(R_p/R_a)/\gamma^*$ at larger values of the Rayleigh number R_a . Christensen and Yuen [29] also indicated that smaller phase transition widths may reduce the value of

$(R_p/R_a)/\gamma^*$ needed for a transition to two-layer convection. Therefore, at larger Rayleigh numbers and smaller values of d , the compositional layering may occur for smaller values of γ^* than those used in this study. The phase transition thicknesses found in these calculations were typically 150–200 km thick. This is perhaps a factor of 30 times too large [9,43].

Caution must be used in applying the results of this study to the Earth's mantle. Hansen and Yuen [44] showed the evolution of double diffusive flow is strongly dependent on the initial conditions. Future studies will at least need to examine the effects of internal heat generation, different initial concentration distributions (especially the size distribution of the light and heavy heterogeneities) and variable viscosity before a definitive answer can be rendered as to whether or not the spinel \rightarrow perovskite + magnesiowustite phase change can induce a compositional boundary in the mantle.

Acknowledgements

Thanks to Mike Gurnis and Don L. Anderson for helpful discussions, Mark Richards for a helpful review and the NCSA at the University of Illinois at Urbana-Champaign for the use of their Cray-2 computer. This research was partly supported by NSF EAR-8957614 and NSF EAR-9005600. S. Weinstein is supported by a 1991 NSF Earth Sciences Postdoctoral Research Fellowship, grant NSF EAR-9102808.

References

- 1 L. Liu, Silicate perovskite from phase transformations of pyrope-garnet at high pressure and temperature, *Geophys. Res. Lett.* 1, 277–280, 1974.
- 2 L. Liu, Post-oxide phases of fosterite and enstatite, *Geophys. Res. Lett.* 2, 417–419, 1975.
- 3 E. Ito and E. Takahashi, Postspinel transformation in the system $Mg_2SiO_4-Fe_2SiO_4$ and some geophysical implications, *J. Geophys. Res.* 94, 10637–10646, 1989.
- 4 E. Ito, M. Akaogi, L. Topor and A. Navrotsky, Negative pressure-temperature slopes for reactions forming $MgSiO_3$ perovskite from calorimetry, *Science* 249, 1275–1278, 1990.
- 5 K.C. Creager and T.H. Jordan, Slab penetration into the lower mantle, *J. Geophys. Res.* 89, 3301–3349, 1984.
- 6 K.C. Creager and T.H. Jordan, Slab penetration into the lower mantle beneath the Mariana and other island arcs of the northwest Pacific, *J. Geophys. Res.* 91, 3572–3589, 1986.
- 7 A.M. Dziewonski and J.H. Woodhouse, Global images of the Earth's interior, *Science* 236, 37–48, 1987.
- 8 R. Van der Hilst, R. Engdahl, W. Spakman, and G. Nolet, Tomographic imaging of subducted lithosphere below northwest Pacific island arcs, *Nature* 353, 37–43.
- 9 M.A. Richards and C.H. Wicks, S-P conversion from the transition zone beneath Tonga and the nature of the 670 km discontinuity, *Geophys. J. Int.* 101, 1–35, 1990.
- 10 J. Revenough and T.H. Jordan, Mantle layering from ScS Reverberations 2. The transition zone, *J. Geophys. Res.* 96, 19763–19780, 1991.
- 11 D.L. Anderson, Chemical inhomogeneity of the mantle, *Earth Planet. Sci. Lett.* 5, 89–94, 1968.
- 12 E.S. Gaffney and D.L. Anderson, Effect of low-spin Fe^{2+} on the composition of the lower mantle, *J. Geophys. Res.* 78, 7005–7014, 1973.
- 13 R. Jeanloz and E. Knittle, Density and composition of the lower mantle, *Philos. Trans. R. Soc. London Ser. A* 328, 377–389, 1989.
- 14 R. Jeanloz and E. Knittle, Reduction of mantle and core properties to a standard state by adiabatic decompression, *Adv. Phys. Geochem.* 6, 275–309, 1986.
- 15 L. Burdick and D.L. Anderson, Interpretation of velocity profiles of the mantle, *J. Geophys. Res.* 80, 1070–1074, 1975.
- 16 A.C. Lees, M.S.T. Bukowski and R. Jeanloz, Reflection properties of phase transition and compositional change models of the 670-km discontinuity, *J. Geophys. Res.* 88, 8145–8159, 1983.
- 17 J.D. Bass and D.L. Anderson, Composition of the upper mantle. Geophysical tests of two petrological models, *Geophys. Res. Lett.* 11, 237–240, 1984.
- 18 R. Jeanloz, Effects of phase transitions and possible composition changes on the seismological structure near 650 km depth, *Geophys. Res. Lett.* 18, 1743–1746, 1991.
- 19 H. Zhou, D.L. Anderson and R.W. Clayton, Modelling of residual spheres for subduction zone earthquakes 1. Apparent slab penetration signatures in the NW Pacific caused by deep diffuse mantle anomalies, *J. Geophys. Res.* 95, 6799–6827, 1990.
- 20 G.F. Davies, Limits on the constitution of the lower mantle, *Geophys. J. R. Astron. Soc.*, 38, 479–503, 1974.
- 21 C.R. Bina and P.G. Silver, Constraints on lower mantle composition and temperature from density and bulk sound velocity profiles, *Geophys. Res. Lett.* 17, 1153–1156, 1990.
- 22 Y. Wang, D.J. Weidner, R.C. Liebermann et al., Phase transition and thermal expansion of $MgSiO_3$ perovskite, *Science* 251, 410–413, 1991.
- 23 A.E. Ringwood, Phase transformations and their bearing on the constitution and dynamics of the mantle, *Geochim. Cosmochim. Acta* 55, 2083–2110.
- 24 D.L. Anderson, Chemical stratification of the mantle, *J. Geophys. Res.* 84, 6297–6298, 1979.
- 25 C.R. Bina and M. Kumazawa, Thermodynamic coupling of phase and chemical boundaries in planetary interiors, *Phys. Earth Planet. Inter.*, submitted, 1992.
- 26 G. Schubert and Turcotte D.L., Phase change and mantle convection, *J. Geophys. Res.* 76, 1424–1428, 1971.

- 27 F.M. Richter and C.E. Johnson, Stability of a chemically layered mantle, *J. Geophys. Res.* 79, 1635–1639, 1974.
- 28 F.M. Richter, Finite amplitude convection through a phase boundary, *Geophys. J.R. Astron. Soc.* 35, 265–276, 1973
- 29 U.R. Christensen and D.A. Yuen, Layered convection induced by phase transitions, *J. Geophys. Res.* 90, 10291–10300, 1985
- 30 P. Machetel and P. Weber, Intermittent layered convection in a model mantle with an endothermic phase change at 670 km, *Nature* 350, 55–57, 1991
- 31 M. Liu, D.A. Yuen, W.L. Zhao and S. Honda, Development of diapiric structures in the upper mantle due to phase transitions, *Science* 252, 1836–1839, 1991
- 32 W.R. Peltier and L.P. Solheim, Mantle phase transitions and layered chaotic convection, *Geophys. Res. Lett.* 19, 321–324, 1992.
- 33 C. Kincaid and P. Olson, Layered mantle convection experiments and the structure of the transition zone, *J. Geophys. Res.*, in press, 1990.
- 34 C. Kincaid and P. Olson, An experimental study of subduction and slab migration, *J. Geophys. Res.* 92, 13832–13840, 1987.
- 35 P. Olson, An experimental approach to thermal convection in a two layered system, *J. Geophys. Res.* 89, 11293–11301, 1984.
- 36 U.R. Christensen and D.A. Yuen, The interaction of a subducting lithospheric slab with a chemical or phase boundary, *J. Geophys. Res.* 89, 4389–4402, 1984.
- 37 U.R. Christensen, Models of mantle convection. one or several layers, *Philos. Trans. R. Soc. London Ser. A* 328, 127–134, 1989.
- 38 L.H. Kellogg, Interaction of plumes with a compositional boundary at 670 km, *Geophys. Res. Lett.* 18, 865–868, 1991.
- 39 L. Stixrude and M.S.T. Bukowski, Stability of (Mg, Fe) SiO_3 perovskite and the structure of the lowermost mantle, *Geophys. Res. Lett.* 19, 1057–1060, 1992.
- 40 S.A. Weinstein, P.L. Olson and D.A. Yuen, Time-dependent large aspect-ratio thermal convection in the Earth's mantle, *Geophys. Astrophys. Fluid Dyn.* 47, 157–197, 1989
- 41 A.W. Hoffman and S.R. Hart, An assessment of the local and regional isotopic equilibria in the mantle, *Earth Planet. Sci. Lett.* 38, 44–62, 1978.
- 42 U. Hansen and D.A. Yuen, Dynamical influences from thermal–chemical instabilities at the core–mantle boundary, *Geophys. Res. Lett.* 16, 629–632, 1989
- 43 E. Ito, E. Takahashi and Y. Matsui, The mineralogy and chemistry of the lower mantle – an implication of the ultra-high-pressure phase relations in the system MgO–FeO–SiO_2 , *Earth Planet. Sci. Lett.* 67, 238–248, 1984.
- 44 U. Hansen and D.A. Yuen, Evolutionary structures in double diffusive convection in magma chambers, *Geophys. Res. Lett.* 14, 1099–1102, 1987.